

Anisotropic Galvanomagnetic Effects in Single Cubic Crystals: A Theory and Its Verification

Yu Miao^{1,*}, Junwen Sun,^{2,3,*} Cunxu Gao¹, Desheng Xue^{1,†} and X. R. Wang^{2,4,‡}

¹Key Laboratory for Magnetism and Magnetic Materials of the Ministry of Education,
Lanzhou University, Lanzhou 730000, China

²Department of Physics, The Hong Kong University of Science and Technology,
Clear Water Bay, Kowloon, Hong Kong, China

³Department of Physics, Nanjing Normal University, Nanjing, China

⁴HKUST Shenzhen Research Institute, Shenzhen 518057, China

 (Received 15 November 2023; revised 22 January 2024; accepted 12 April 2024; published 15 May 2024)

A theory of anisotropic galvanomagnetic effects in single cubic crystals and its experimental verifications are presented for the current in the (001) plane. In contrast to the general belief that galvanomagnetic effects in single crystals are highly sensitive to many internal and external effects and have no universal features, the theory predicts universal angular dependencies of longitudinal and transverse resistivity and various characteristics when magnetization rotates in the (001) plane, the plane perpendicular to the current, and the plane containing the current and [001] direction. The universal angular dependencies are verified by experiments on Fe₃₀Co₇₀ single cubic crystal film. The findings provide new avenues for fundamental research and applications of galvanomagnetic effects, because single crystals offer advantages over polycrystalline materials for band structure and crystallographic orientation engineering.

DOI: [10.1103/PhysRevLett.132.206701](https://doi.org/10.1103/PhysRevLett.132.206701)

Anisotropic magnetoresistance (AMR) is a well-known phenomenon that was first discovered in 1856 by Kelvin [1]. AMR refers to dependences of the longitudinal resistivity on magnetization direction while the dependences of the transverse resistivity on the magnetization direction are referred to as the anomalous Hall effect (AHE) and planar Hall effect (PHE) in the Hall geometry. AHE and PHE are, respectively, referred to as dependences on the perpendicular and in-plane (to the Hall plane) components of the magnetization. AMR, AHE, and PHE have been extensively studied in magnetic polycrystalline materials [2–5] and single crystals [6–10] and their complete understanding is a problem that has persisted for more than 150 years in the field of magnetism.

The universal angular dependencies of longitudinal and transverse resistivity in magnetic polycrystalline materials are well known [11–14], which says $\rho_{xx}(\alpha) = \rho_0 + A_0 \cos^2 \alpha$ and $\rho_{xy}(\alpha) = (A_0/2) \sin 2\alpha$, where α is the angle between the magnetization and current [15–19]. For galvanomagnetic effects in single crystals, there are also many studies [20–28] that show complicated behaviors [7,8]. However, despite the known roles of spin-orbit interaction, spin-dependent scatterings, and electron interactions with crystallographic directions in galvanomagnetic effects [11,12], no universal angular dependencies of longitudinal and transverse resistivity in magnetic single crystals have been found to date.

The study of galvanomagnetic effects in single crystals is important for several reasons. First, it should deepen our

understanding of the fundamental physics of magnetoresistance, including the role of crystal symmetry and electronic structure. In single crystals, galvanomagnetic effects are directional [29], because electronic structures are different along different crystallographic directions, leading to different electron scattering and different group velocities. Second, it enables the development of new materials with tailored magnetic and electronic properties, which can be useful for applications in spintronics such as magnetic recording and sensing [11,12]. The in-plane AMR in single crystals has demonstrated higher-order symmetry [7] and phase shift [30] beyond polycrystalline materials, which may serve as an opportunity for discovering new effects.

In this Letter, the theory based on vector order parameters for galvanomagnetic effects in single cubic crystals is presented. Through the transport measurements on Fe₃₀Co₇₀ single cubic crystal film when the current is in the (001) plane with the magnetization rotated in the (001) plane, the plane perpendicular to the current, and the plane containing the current and the [001] direction, the universal angular dependencies of longitudinal and transverse resistivity are verified. We find that only 8 parameters are needed to describe all longitudinal and transverse resistivity curves below the 4th order. We also predict several characteristics of galvanomagnetic effects, such as that the transverse resistivity with current along the [100] and [110] directions is identical when the magnetization is rotating in the above three planes. Our results provide new insights of galvanomagnetic effects in single crystals.

In ferromagnetic single crystals, the scattering of electrons is related to crystallographic directions, which can be characterized by three crystalline axes $\vec{n}_1, \vec{n}_2, \vec{n}_3$, and the magnetization \vec{M} whose magnitude is a constant and direction is along \vec{m} . In the linear response region, the electric field \vec{E} in response to an applied current density \vec{J} in a crystal must be

$$\vec{E} = \overleftrightarrow{\rho}(\vec{m}, \vec{n}_1, \vec{n}_2, \vec{n}_3)\vec{J}, \quad (1)$$

where $\overleftrightarrow{\rho}(\vec{m}, \vec{n}_1, \vec{n}_2, \vec{n}_3)$ is a Cartesian tensor of rank 2. Although the tensor values depend on microscopic properties of the crystal and parameters that defines its thermodynamic state, tensor $\overleftrightarrow{\rho}$ can be constructed only by $\vec{m}, \vec{n}_1, \vec{n}_2$, and \vec{n}_3 . There are ten possible Cartesian tensors: $\vec{m}\vec{m}, \vec{n}_1\vec{n}_1, \vec{n}_2\vec{n}_2, \vec{n}_3\vec{n}_3, \vec{m}\vec{n}_1, \vec{m}\vec{n}_2, \vec{m}\vec{n}_3, \vec{n}_1\vec{n}_2, \vec{n}_1\vec{n}_3$, and $\vec{n}_2\vec{n}_3$. Each of them, however, is reducible [31], and can be decomposed into the direct sum of a scalar, a vector, and a traceless symmetric tensor. Then it is possible to construct seven vectors and ten traceless symmetric tensors of ranks 2: $\vec{m}, \vec{n}_1, \vec{n}_2, \vec{n}_3, \vec{m} \times \vec{n}_i, \vec{m}\vec{m}-1/3, \vec{m}\vec{n}_i + \vec{n}_i\vec{m} - 2\vec{m} \cdot \vec{n}_i/3$, and $\vec{n}_i\vec{n}_j + \vec{n}_j\vec{n}_i - 2\vec{n}_j \cdot \vec{n}_i/3$ ($i, j = 1, 2, 3$). Thus, $\overleftrightarrow{\rho}$ should be the linear combination of 17 direction-dependent terms together with a scalar term. The electric field \vec{E} induced by \vec{J} , after grouping similar terms, must take the following most generic form

$$\begin{aligned} \vec{E} = & \rho_0\vec{J} + \left(B_0\vec{m} + \sum_{i=1}^3 B_i\vec{n}_i + \sum_{i=1}^3 B_{3+i}\vec{m} \times \vec{n}_i \right) \times \vec{J} \\ & + \sum_{i=1}^3 A_i[(\vec{J} \cdot \vec{m})\vec{n}_i + (\vec{J} \cdot \vec{n}_i)\vec{m}] + \sum_{i=1}^3 A_{i+3}(\vec{J} \cdot \vec{n}_i)\vec{n}_i \\ & + A_7[(\vec{J} \cdot \vec{n}_1)\vec{n}_2 + (\vec{J} \cdot \vec{n}_2)\vec{n}_1] + A_8[(\vec{J} \cdot \vec{n}_1)\vec{n}_3 \\ & + (\vec{J} \cdot \vec{n}_3)\vec{n}_1] + A_9[(\vec{J} \cdot \vec{n}_2)\vec{n}_3 + (\vec{J} \cdot \vec{n}_3)\vec{n}_2] \\ & + A_0(\vec{J} \cdot \vec{m})\vec{m}, \end{aligned} \quad (2)$$

where ρ_0, A_k ($k = 0, \dots, 9$), and B_l ($l = 0, \dots, 6$) are parameters that are determined by the extrinsic and intrinsic properties of a sample such as the temperature, disorders, and band structures. Of course, these parameters can, in principle, depend on the scalars constructed from \vec{m} and \vec{n}_i . Among them, only $\vec{m} \cdot \vec{n}_i \equiv m_i$ ($i = 1, 2, 3$) can introduce the anisotropic effect. For crystals with reciprocity, \vec{E} should be the same under $\vec{n}_i \rightarrow -\vec{n}_i$ transformations. Thus, $\rho_0, A_0, A_4, A_5, A_6$, and B_0 must be even functions of m_i ($i = 1, 2, 3$). A_i, B_i , and B_{i+3} must be odd in m_i and even in $m_{j \neq i}$ ($i = 1, 2, 3$) while A_7 is odd in m_1 and m_2 , and even in m_3 . For example, $\rho_0 = \sum_{p,q,r} \rho_{0pqr} m_1^{2p} m_2^{2q} m_3^{2r}$

and $A_1 = \sum_{p,q,r} A_{1pqr} m_1^{2p+1} m_2^{2q} m_3^{2r}$. Expansion coefficients ρ_{0pqr} and A_{1pqr} measure the $2(p+q+r)$ -th order and $2(p+q+r)+1$ -th order interactions of electrons with magnetization and crystal order parameters, respectively, because the A_1 term contains already one \vec{m} . Similar expansions can be done for other A 's and B 's, see Supplemental Material [32]. Because magnetic interactions are usually weak, we shall keep our analysis below the 4th order of electron-magnetization interactions.

Equation (2) is the most general electric field response of a crystal to an external current. Among all possible physical quantities, AMR and PHE of a given crystal can be obtained directly from it. In the absence of \vec{n}_i such as polycrystalline or amorphous magnets, Eq. (2) reduces to the well-known generalized Ohm's law of polycrystalline materials [17,18] with only ρ_0, B_0 , and A_0 terms. The B_0 term is the usual anomalous Hall effect, and the A_0 term is the AMR and PHE for ferromagnetic polycrystalline. If current \vec{J} is defined as the x axis and the Hall bar is in the xy plane throughout this Letter, the longitudinal and transverse resistivity are $\rho_{xx} = \rho_0 + A_0 \cos^2 \alpha$ and $\rho_{xy} = B_0 m_z + (A_0/2) \sin 2\alpha$, where α is the angle between \vec{m} and \vec{J} . Obviously, ρ_0 is the longitudinal resistivity when \vec{J} is perpendicular to \vec{m} and B_0 is the anomalous Hall coefficient. A_0 is the amplitude of the conventional AMR and PHE that is typically a few percent of ρ_0 . Interestingly, the tensor analysis leads to the famous Einstein gravitation field theory [33]. The analysis has also been successfully used to predict anomalous spin Hall effects [34–36] and unusual AMR in bilayers [37].

In order to see the implications of Eq. (2), we apply it to cubic crystals. In this Letter, a widely used configuration in experiments is considered, where the (001) plane lies on the xy plane, the z axis is along the [001] direction, and \vec{n}_1, \vec{n}_2 , and \vec{n}_3 are equivalent and mutually orthogonal with each other corresponding to the [100], [010], and [001] directions. According to Eq. (2), the longitudinal and transverse resistivity are $\rho_{xx}^\theta \equiv \vec{E} \cdot \hat{x}/J = \rho_0 + A_0 m_x^2 + \sum_{i=1}^2 (2A_i m_x n_{ix} + A_{i+3} n_{ix}^2) + A_7 n_{1x} n_{2x}$ and $\rho_{xy}^\theta \equiv \vec{E} \cdot \hat{y}/J = B_0 m_z + B_3 + B_4 (m_x n_{1y} - m_y n_{1x}) + B_5 (m_x n_{2y} - m_y n_{2x}) + A_0 m_x m_y + \sum_{i=1}^2 [A_i (m_x n_{iy} + m_y n_{ix}) + A_{i+3} n_{ix} n_{iy}] + A_7 (n_{1x} n_{2y} + n_{1y} n_{2x})$, where θ is the angle between the [100] direction and the x axis.

Following the convention in literature, we define α as the angle between \vec{m} and \vec{J} when \vec{m} rotates in the xy plane, β and γ as the angles between \vec{m} and the z axis when \vec{m} rotates in the yz and zx planes, respectively, as illustrated in Fig. 1(a). After some tedious algebra, as shown in the Supplemental Material [32], the angular dependencies of ρ_{xx}^θ and ρ_{xy}^θ , with terms not higher than m_i^4 , are

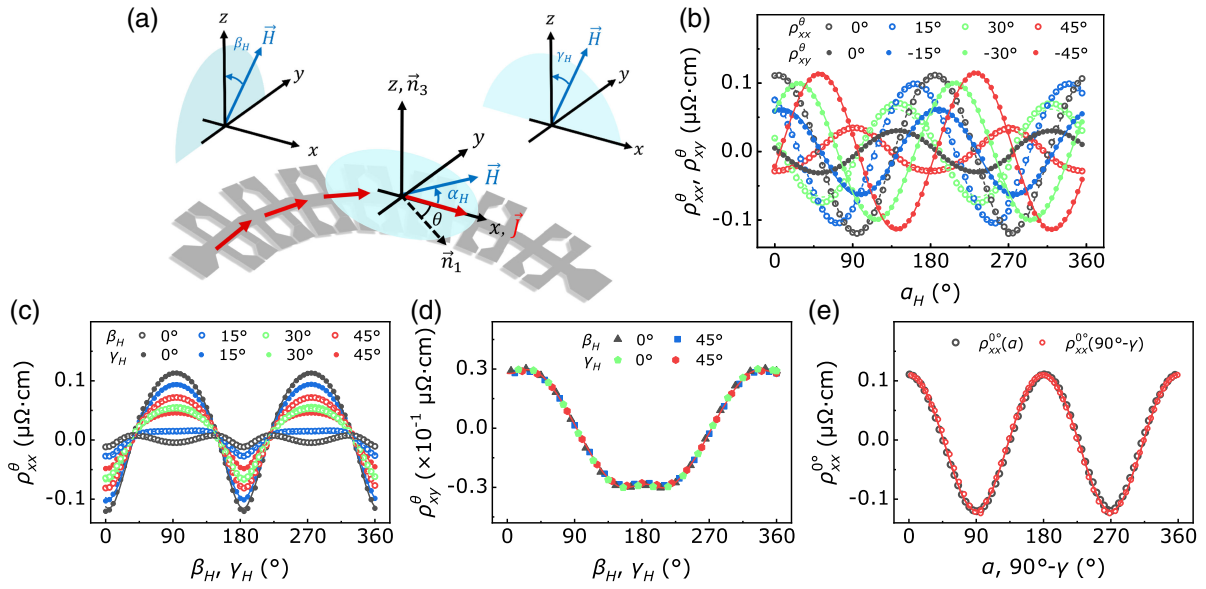


FIG. 1. The longitudinal and transverse resistivity of Fe₃₀Co₇₀ single cubic crystal film under 6 T field. (a) The schematics of the experimental setup. Current \vec{J} is along the x axis in the (001) plane. θ is the angle between \vec{J} and \vec{n}_1 , and z axis is along the [001] direction. α_H is the angle between the magnetic field \vec{H} and the x axis when \vec{H} is in the (001) plane. β_H and γ_H are the angles between \vec{H} and the z axis when \vec{H} is in the yz and zx planes, respectively. (b) $\rho_{xx}^\theta(\alpha_H)$ (open circles) and $\rho_{xy}^\theta(\alpha_H)$ (solid circles) for $\theta = 0^\circ, \pm 15^\circ, \pm 30^\circ$, and $\pm 45^\circ$. The dotted (solid) lines are the fitting curves by Eq. (3) with $\alpha = \alpha_H$. (c) $\rho_{xx}^\theta(\beta_H)$ (open circles) and $\rho_{xx}^\theta(\gamma_H)$ (solid circles) for $\theta = 0^\circ, 15^\circ, 30^\circ$, and 45° . The dotted (solid) lines are the fitting curves by Eq. (3) with $\beta(\gamma) = \beta_H(\gamma_H) + \delta$. δ is the angle of magnetization deviated from magnetic field. (d) $\rho_{xy}^\theta(\beta_H)$ (black and blue circles) and $\rho_{xy}^\theta(\gamma_H)$ (green and red circles) for $\theta = 0^\circ$ and 45° . The solid lines are the fitting curves by Eqs. (4) and (5) with $\beta(\gamma) = \beta_H(\gamma_H) + \delta$. To display experimental data clearly, only one data point is shown for every four data points collected. (e) $\rho_{xx}^{0^\circ}(\alpha)$ (open black circles) and $\rho_{xx}^{0^\circ}(90^\circ - \gamma)$ (open red circles): They are overlapped with each other and agree with Eq. (4) (solid line).

$$\begin{aligned}
 \rho_{xx}^\theta(\alpha) &= \rho_1 \cos 2\alpha + \rho_2 \cos(2\alpha + 4\theta) + \rho_3 \cos(4\alpha + 4\theta), \\
 \rho_{xx}^\theta(\beta) &= (\mu_1 - \mu_1 \cos 4\theta) \cos 2\beta + (\rho_4 + \rho_5 \cos 4\theta) \cos 4\beta, \\
 \rho_{xx}^\theta(\gamma) &= (\mu_2 + \mu_3 \cos 4\theta) \cos 2\gamma + (\mu_4 + \mu_5 \cos 4\theta) \cos 4\gamma, \\
 \rho_{xy}^\theta(\alpha) &= \rho_1 \sin 2\alpha - \rho_2 \sin(2\alpha + 4\theta) - \rho_6 \sin(4\alpha + 4\theta), \\
 \rho_{xy}^\theta(\beta) &= \rho_7 \cos \beta + \sin 4\theta (\mu_6 \cos 2\beta + \mu_7 \cos 4\beta) + \rho_8 \cos 3\beta, \\
 \rho_{xy}^\theta(\gamma) &= \rho_7 \cos \gamma + \sin 4\theta (\mu_8 \cos 2\gamma + \mu_9 \cos 4\gamma) + \rho_8 \cos 3\gamma,
 \end{aligned} \tag{3}$$

where ρ_i ($i = 1, 2, \dots, 8$) are the only independent constants that depend on material parameters. μ_i ($i = 1, 2, \dots, 9$) are linear combinations of ρ_i ($i = 1, 2, \dots, 8$) and are $\mu_1 = -(\rho_2 - \rho_3)/2$, $\mu_2 = \mu_1 - \rho_1$, $\mu_3 = \mu_1 - \rho_3$, $\mu_4 = 3\rho_3/4 + \rho_5$, $\mu_5 = \rho_3 - \mu_4$, $\mu_6 = -(\rho_2 - \rho_6)/2$, $\mu_7 = \rho_3/8 - \rho_5 + \rho_6/8$, $\mu_8 = \mu_6 + \rho_2$, $\mu_9 = -\rho_6/4 - \mu_7$. We have also removed the angular independent background resistance such that averaged $\rho_{xx}^\theta(\alpha)$ with respect to α is zero. It should be emphasized that the angular dependences of galvanomagnetic effects are fully determined by these 8 coefficients. ρ_1 describes the usual twofold AMR and PHE while ρ_7 is the usual AHE.

For \vec{J} along [100] ($\theta = 0^\circ$) and [110] ($\theta = 45^\circ$ and equivalent to $\theta = -45^\circ$ or $[\bar{1}\bar{1}0]$), we have

$$\begin{aligned}
 \rho_{xx}^{0^\circ}(\alpha) &= (\rho_1 + \rho_2) \cos 2\alpha + \rho_3 \cos 4\alpha, \\
 \rho_{xx}^{0^\circ}(\beta) &= (\rho_4 + \rho_5) \cos 4\beta, \\
 \rho_{xx}^{0^\circ}(\gamma) &= -(\rho_1 + \rho_2) \cos 2\gamma + \rho_3 \cos 4\gamma, \\
 \rho_{xy}^{0^\circ}(\alpha) &= (\rho_1 - \rho_2) \sin 2\alpha - \rho_6 \sin 4\alpha, \\
 \rho_{xy}^{0^\circ}(\beta) &= \rho_7 \cos \beta + \rho_8 \cos 3\beta, \\
 \rho_{xy}^{0^\circ}(\gamma) &= \rho_7 \cos \gamma + \rho_8 \cos 3\gamma,
 \end{aligned} \tag{4}$$

and

$$\begin{aligned}
 \rho_{xx}^{45^\circ}(\alpha) &= (\rho_1 - \rho_2) \cos 2\alpha - \rho_3 \cos 4\alpha, \\
 \rho_{xx}^{45^\circ}(\beta) &= (\rho_3 - \rho_2) \cos 2\beta + (\rho_4 - \rho_5) \cos 4\beta, \\
 \rho_{xx}^{45^\circ}(\gamma) &= (\rho_3 - \rho_1) \cos 2\gamma + \left(\frac{1}{2}\rho_3 + 2\rho_5\right) \cos 4\gamma, \\
 \rho_{xy}^{45^\circ}(\alpha) &= (\rho_1 + \rho_2) \sin 2\alpha + \rho_6 \sin 4\alpha, \\
 \rho_{xy}^{45^\circ}(\beta) &= \rho_7 \cos \beta + \rho_8 \cos 3\beta, \\
 \rho_{xy}^{45^\circ}(\gamma) &= \rho_7 \cos \gamma + \rho_8 \cos 3\gamma.
 \end{aligned} \tag{5}$$

Interestingly, there are several characteristics according to Eqs. (4) and (5). (i) The amplitude of the twofold in $\rho_{xx}^{0^\circ(45^\circ)}(\alpha)$ is equal to that in $\rho_{xy}^{45^\circ(0^\circ)}(\alpha)$, and the amplitude of the fourfold in $\rho_{xx(xy)}^{0^\circ}(\alpha)$ and $\rho_{xx(xy)}^{45^\circ}(\alpha)$ are always the same. In fact, this fourfold amplitude of ρ_3 does not depend on θ , and this is exactly what was observed in $L1_0$ FePt films [38]. (ii) $\rho_{xx}^{0^\circ}(\beta)$ have no twofold symmetry but strictly fourfold symmetry. (iii) The results of $\rho_{xy}^{0^\circ}(\beta)$, $\rho_{xy}^{0^\circ}(\gamma)$, $\rho_{xy}^{45^\circ}(\beta)$, and $\rho_{xy}^{45^\circ}(\gamma)$ which only have a onefold and threefold term are identical, and $\rho_{xx}^{0^\circ}(90^\circ - \gamma)$ is identical to $\rho_{xx}^{0^\circ}(\alpha)$. Furthermore, the sum of amplitudes of the twofold terms in $\rho_{xx}^{0^\circ(45^\circ)}(\alpha)$ and $\rho_{xx}^{0^\circ(45^\circ)}(\gamma)$ equals to that in $\rho_{xx}^{0^\circ(45^\circ)}(\beta)$. Other relationships among the angular dependencies of longitudinal and transverse resistivity also exist and can be used to test the theory. By inspection, early experiments of AMR and PHE in Refs. [23] and [7] for (Ga, Mn)As and $\text{Co}_x\text{Fe}_{1-x}$ single cubic crystal films along these two special angles agree with our theory. Moreover, the tensor analysis includes all possible microscopic mechanisms such as spin Hall magnetoresistance [39], Rashba-Edelstein magnetoresistance [40], and anomalous Hall magnetoresistance [41].

To verify the theory presented above, we measured angular dependences of ρ_{xx}^θ and ρ_{xy}^θ of $\text{Fe}_{30}\text{Co}_{70}$ single crystal film. A 19-nm-thick $\text{Fe}_{30}\text{Co}_{70}$ single crystal film was grown on MgO(001) substrate at room temperature by molecular beam epitaxy. The single crystal sample is patterned into Hall bars along different crystallographic direction using photolithography and ion beam etching as schematically shown in Fig. 1(a). In one batch, we fabricated Hall bars along $\theta = 0^\circ, \pm 15^\circ, \pm 30^\circ$, and $\pm 45^\circ$ with size of $1000 \mu\text{m} \times 50 \mu\text{m}$. Both the longitudinal and transverse resistivity ρ_{xx}^θ and ρ_{xy}^θ are measured using the four-probe method. All measurements were performed at room temperature. The results for current in the (001) plane of our $\text{Fe}_{30}\text{Co}_{70}$ film are plotted in Figs. 1(b)–1(d). The symbols are experimental data (after subtracting the background resistances, and ρ_{xy}^θ divided by a coefficient of 1.19 due to the effect of the finite electrode size for the Hall measurement [7,30]). The average sheet resistivity of our films along $\theta = 30^\circ$ is $8.82 \mu\Omega\text{cm}$, and a variation of $8.82 \pm 0.47 \mu\Omega\text{cm}$ along different crystallographic directions exists. In order to compare the experimental results with the theoretical prediction, α , β , and γ of magnetization should be derived from the corresponding angles α_H , β_H , and γ_H of magnetic field which can be determined experimentally. A 6 T magnetic field is applied to ensure the magnetization close to the direction of field. Then $\alpha \simeq \alpha_H$ because of the magnitude of in-plane magnetocrystalline anisotropy field is 2 orders of magnitude smaller than the applied field strength. $\beta \simeq \beta_H + \delta$ and $\gamma \simeq \gamma_H + \delta$ since the out-of-plane shape anisotropy field is about 2 T which is not much smaller than 6 T. The angle δ of magnetization

TABLE I. The fitting parameters in Eq. (3) for Figs. 1(b)–1(d).

$\times 10^{-2}$	ρ_1	ρ_2	ρ_3	ρ_4
$\mu\Omega\text{cm}$	4.185	7.337	-0.446	-0.653
	ρ_5	ρ_6	ρ_7	ρ_8
$\mu\Omega\text{cm}$	-0.145	-0.104	3.452	-0.650

deviated from the magnetic field can be expressed as [42,43]

$$\delta(\beta_H) = \frac{\sin 2\beta_H}{2(H/H_K - \cos 2\beta_H)}, \quad (6)$$

where H is the magnitude of magnetic field, and H_K is the anisotropy field. Equation (6) is also applicable to γ_H . The dashed and solid lines in Figs. 1(b)–1(d) are fitting curves by Eq. (3) with 8 fitting constants given in Table I after converting α , β , and γ to α_H , β_H , and γ_H .

The characteristics of single cubic crystals from the theory can be verified experimentally. Figure 1(b) shows ρ_{xx} and ρ_{xy} in the xy plane. The amplitude of ρ_{xx} gradually decreases while that of ρ_{xy} increases with current applied from $\theta = 0^\circ$ to $\theta = 45^\circ$. The amplitudes of $\rho_{xy}^{45^\circ(0^\circ)}(\alpha)$ and $\rho_{xx}^{0^\circ(45^\circ)}(\alpha)$ are the same as predicted. Figure 1(c) shows ρ_{xx} in the yz and the zx plane. A fourfold term appears in $\rho_{xx}^{0^\circ}(\beta)$ as predicted by the theory. Figure 1(d) shows ρ_{xy} in the yz and the zx plane. All four $\rho_{xy}^\theta(\beta)$ and $\rho_{xy}^\theta(\gamma)$ for $\theta = 0^\circ$ and 45° are coincident. Figure 1(e) shows ρ_{xx} in terms of α and $(90^\circ - \gamma)$ using the angle conversions mentioned above. $\rho_{xx}^{0^\circ}(90^\circ - \gamma)$ and $\rho_{xx}^{0^\circ}(\alpha)$ are the same as predicted by our theory. Our experimental measurements support unambiguously all characteristics summarized early.

To have a better picture of how ρ_{xx} and ρ_{xy} vary with the current direction (θ) and the direction of \vec{m} , we convert α_H , β_H , and γ_H to α , β , and γ , and plot ρ_{xx}^θ and ρ_{xy}^θ as functions of θ and α , or β , or γ in Fig. 2. The three-dimensional surfaces are the theoretical formula of Eq. (3) with parameters given in Table I. The beautiful agreements of experiments and theory in the 3D plots are a strong testimony of correctness of the theory, meaning clearly that only 8 independent parameters can indeed describe all longitudinal and transverse resistivity curves.

To test how good our field and magnetization direction correction is, we also measure AMR at different fields with current applied along the [100] crystallographic direction. Figure 3 is $\rho_{xx}^{0^\circ}(\beta_H)$ (a) and $\rho_{xx}^{0^\circ}(\gamma_H)$ (b) for field at 3 T (red squares), 6 T (green circles), and 9 T (blue triangles). Although the AMR curves are significantly different with increasing fields, especially around $\beta_H(\gamma_H) = 22.5^\circ$, the results can also be well fitted by Eqs. (4) with the same parameters in Table I, revealing the field independence of

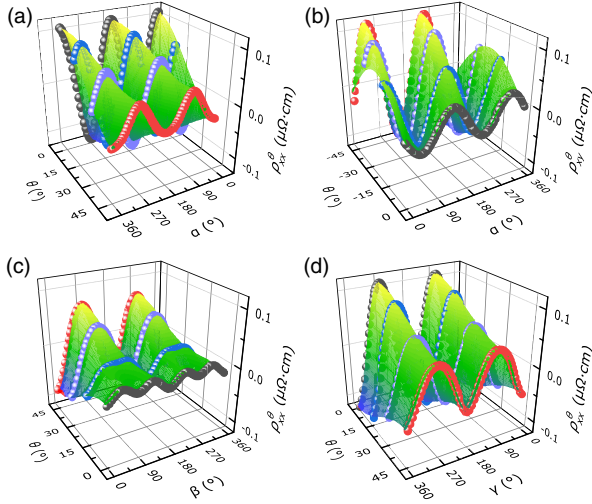


FIG. 2. Three-dimensional plots of ρ_{xx} and ρ_{xy} as functions of current and magnetization directions when the current is in the (001) plane. Symbols are experimental data of ρ_{xx} [(a), (c), (d)] and ρ_{xy} (b) in terms of θ and α [(a) and (b)], θ and β (c), and θ and γ (d). The space curved surfaces are Eq. (3) with ρ_i ($i = 1, 2, \dots, 8$) given in Table I.

the 8 parameters as suggested by the theory. Of course, the angles in Eqs. (3) are converted to β_H and γ_H by Eq. (6).

It must be mentioned that there are fundamental differences between current tensor analysis and the symmetry consideration [3,44,45] widely used to understand AMR in single crystals. Although the symmetry consideration is not wrong, it does not reveal universal angular dependencies of ρ_{xx} and ρ_{xy} and possible identities. One obtains different results presented here when the symmetry analysis is applied on a cubic crystal [8]. In fact, it cannot even recover the universal behavior of ρ_{xx} and ρ_{xy} in polycrystalline without extra inputs [8]. One recent progress connects AMR with the magnetization-dependent band structure near the Fermi level [7,9]. These density functional calculations are consistent with our theory although they cannot identify universal angular dependencies and characteristics in ρ_{xx} and ρ_{xy} .

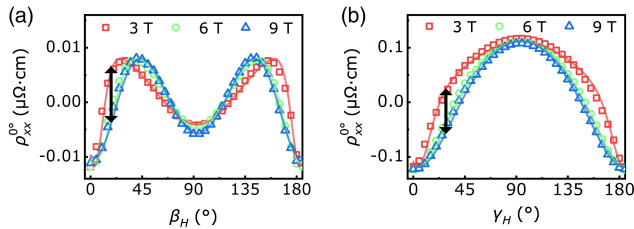


FIG. 3. AMR with current along $\theta = 0^\circ$ under different magnetic fields. $\rho_{xx}^{0^\circ}$ vs β_H (a) and γ_H (b) for magnetic fields of 3, 6, and 9 T. Symbols are the experimental data, and the solid lines are Eq. (4). The black bidirectional arrow is used to indicate differences between the curves.

In summary, a theory of angular dependency of generic galvomagnetic effects for single cubic crystals are presented. Only 8 independent and intrinsic parameters are needed to describe angular dependencies of magnetoresistance. These parameters are intrinsic because they must exist in all single cubic crystals. A set of characteristics among ρ_{xx}^θ and ρ_{xy}^θ are predicted for current along the [100] and [110] directions and the magnetization rotating in the xy , xz , and yz planes. The predictions are beautifully verified by the experiments on $\text{Fe}_{30}\text{Co}_{70}$ single cubic crystal film. We believe that the long-standing issue of universal angular dependencies of galvomagnetic effects in single cubic crystals is resolved.

This work is supported by the National Key Research and Development Program of China (No. 2020YFA0309600), the National Natural Science Foundation of China Grants (No. 91963201, No. 12374122, No. 12174163, and No. 12074157), and Hong Kong Research Grants Council Grants (No. 16302321, No. 16300522, and No. 16300523).

*These authors contributed equally to this work.

[†]xueds@lzu.edu.cn

[‡]phxwan@ust.hk

- [1] W. Thomson, On the electro-dynamic qualities of metals: Effects of magnetization on the electric conductivity of nickel and of iron, *Proc. R. Soc. London* **8**, 546 (1857).
- [2] J. Smit, Magnetoresistance of ferromagnetic metals and alloys at low temperatures, *Physica (Amsterdam)* **17**, 612 (1951).
- [3] T. R. McGuire and R. Potter, Anisotropic magnetoresistance in ferromagnetic 3d alloys, *IEEE Trans. Magn.* **11**, 1018 (1975).
- [4] T. R. McGuire, J. A. Aboafand, and E. Klokholm, Negative anisotropic magnetoresistance in 3d metals and alloys containing iridium, *IEEE Trans. Magn.* **20**, 972 (1984).
- [5] R. C. O'Handley, Spontaneous Hall effect and resistivity of Fe-Co-Ni-base glasses, *Phys. Rev. B* **18**, 2577 (1978).
- [6] P. Wisniewski, Giant anisotropic magnetoresistance and magnetothermopower in cubic 3:4 uranium pnictides, *Appl. Phys. Lett.* **90**, 192106 (2007).
- [7] F. L. Zeng, Z. Y. Ren, Y. Li, J. Y. Zeng, M. W. Jia, J. Miao, A. Hoffmann, W. Zhang, Y. Z. Wu, and Z. Yuan, Intrinsic mechanism for anisotropic magnetoresistance and experimental confirmation in $\text{Co}_x\text{Fe}_{1-x}$ single-crystal films, *Phys. Rev. Lett.* **125**, 097201 (2020).
- [8] L. Nadvornik, M. Borchert, L. Brandt, R. Schlitz, K. A. de Mare, K. Vyborny, I. Mertig, G. Jakob, M. Klau, S. T. B. Goennenwein, M. Wolf, G. Woltersdorf, and T. Kampfrath, Broadband terahertz probes of anisotropic magnetoresistance disentangle extrinsic and intrinsic contributions, *Phys. Rev. X* **11**, 021030 (2021).
- [9] G. E. W. Bauer, Anisotropic magnetoresistance: A 170-year-old puzzle solved, *Sci. China Phys. Mech. Astron.* **64**, 217531 (2021).
- [10] A. A. Starikov, Y. Liu, Z. Yuan, and P. J. Kelly, Calculating the transport properties of magnetic materials from

- first principles including thermal and alloy disorder, noncollinearity, and spin-orbit coupling, *Phys. Rev. B* **97**, 214415 (2018).
- [11] I. A. Campbell and A. Fert, Transport properties of ferromagnets, in *Handbook of Ferromagnetic Materials* (Elsevier, New York, 1982).
- [12] R. C. O'Handley, *Modern Magnetic Materials: Principles and Applications* (Wiley, New York, 2000).
- [13] I. A. Campbell, A. Fert, and O. Jaoul, The spontaneous resistivity anisotropy in Ni-based alloys, *J. Phys. C* **3**, S95 (1970).
- [14] S. Kokado, M. Tsunoda, K. Harigaya, and A. Sakuma, Anisotropic magnetoresistance effects in Fe, Co, Ni, Fe₄N, and half-metallic ferromagnet: A systematic analysis, *J. Phys. Soc. Jpn.* **81**, 024705 (2012).
- [15] S. Kokado and M. Tsunoda, Anisotropic magnetoresistance effect: General expression of AMR ratio and intuitive explanation for sign of AMR ratio, *Adv. Mater. Res.* **750**, 978 (2013).
- [16] E. De Ranieri, A. W. Rushforth, K. Vyborny, U. Rana, E. Ahmad, R. P. Campion, C. T. Foxon, B. L. Gallagher, A. C. Irvine, J. Wunderlich, and T. Jungwirth, Lithographically and electrically controlled strain effects on anisotropic magnetoresistance in (Ga,Mn)As, *New J. Phys.* **10**, 065003 (2008).
- [17] Y. Zhang, H. W. Zhang, and X. R. Wang, Extraordinary galvanomagnetic effects in polycrystalline magnetic films, *Europhys. Lett.* **113**, 47003 (2016).
- [18] Y. Zhang, X. S. Wang, H. Y. Yuan, S. S. Kang, H. W. Zhang, and X. R. Wang, Dynamic magnetic susceptibility and electrical detection of ferromagnetic resonance, *J. Phys. Condens. Matter* **29**, 095806 (2017).
- [19] Y. Zhang, Q. Liu, B. F. Miao, H. F. Ding, and X. R. Wang, Anatomy of electrical signals and dc-voltage line shape in spin-torque ferromagnetic resonance, *Phys. Rev. B* **99**, 064424 (2019).
- [20] M. Tondra, D. K. Lottis, K. T. Riggs, Y. Chen, E. D. Dahlberg, and G. A. Prinz, Thickness dependence of the anisotropic magnetoresistance in epitaxial iron films, *J. Appl. Phys.* **73**, 6393 (1993).
- [21] R. P. van Gorkom, J. Caro, T. M. Klapwijk, and S. Radelaar, Temperature and angular dependence of the anisotropic magnetoresistance in epitaxial Fe films, *Phys. Rev. B* **63**, 134432 (2001).
- [22] W. Limmer, M. Glunk, J. Daeubler, T. Hummel, W. Schoch, R. Sauer, C. Bihler, H. Huebl, M. S. Brandt, and S. T. B. Goennenwein, Angle-dependent magnetotransport in cubic and tetragonal ferromagnets: Application to (001)- and (113)A-oriented (Ga,Mn)As, *Phys. Rev. B* **74**, 205205 (2006).
- [23] D. Wu, P. Wei, E. Johnston-Halperin, D. D. Awschalom, and Jing Shi, High-field magnetocrystalline anisotropic resistance effect in (Ga,Mn)As, *Phys. Rev. B* **77**, 125320 (2008).
- [24] W. Limmer, J. Daeubler, L. Dreher, M. Glunk, W. Schoch, S. Schwaiger, and R. Sauer, Advanced resistivity model for arbitrary magnetization orientation applied to a series of compressive- to tensile-strained (Ga,Mn)As layers, *Phys. Rev. B* **77**, 205210 (2008).
- [25] Y. Bason, J. Hoffman, C. H. Ahn, and L. Klein, Magnetoresistance tensor of La_{0.8}Sr_{0.2}MnO₃, *Phys. Rev. B* **79**, 092406 (2009).
- [26] N. Naftalis, A. Kaplan, M. Schultz, C. A. F. Vaz, J. A. Moyer, C. H. Ahn, and L. Klein, Field-dependent anisotropic magnetoresistance and planar Hall effect in epitaxial magnetite thin films, *Phys. Rev. B* **84**, 094441 (2011).
- [27] Z. Ding, J. X. Li, J. Zhu, T. P. Ma, C. Won, and Y. Z. Wu, Three-dimensional mapping of the anisotropic magnetoresistance in Fe₃O₄ single crystal thin films, *J. Appl. Phys.* **113**, 17B103 (2013).
- [28] T. Hupfauer, A. Matos-Abiague, M. Gmitra, F. Schiller, J. Loher, D. Bougeard, C. H. Back, J. Fabian, and D. Weiss, Emergence of spin-orbit fields in magnetotransport of quasi-two-dimensional iron on gallium arsenide, *Nat. Commun.* **6**, 7374 (2015).
- [29] Y. Miao, T. Li, X. Chen, C. X. Gao, and D. S. Xue, Temperature dependence of angular-dependent magnetoresistance in epitaxial Fe(001) film, *J. Appl. Phys.* **133**, 103902 (2023).
- [30] F. L. Zeng, C. Zhou, M. W. Jia, D. Shi, Y. Huo, W. Zhang, and Y. Z. Wu, Strong current-direction dependence of anisotropic magnetoresistance in single crystalline Fe/GaAs(110) films, *J. Magn. Magn. Mater.* **499**, 166204 (2020).
- [31] J. J. Sakurai/San Fu Tuan, *Modern Quantum Mechanics (Revised Edition)* (Addison Wesley Longman, Reading, MA, 1994).
- [32] See Supplemental Material at <http://link.aps.org/supplemental/10.1103/PhysRevLett.132.206701> for the derivation of the expressions of ρ_{xx} and ρ_{xy} with respect to m_i and angles, the results considering the linear dependence of other parameters, and the structural characterization of Fe₃₀Co₇₀ film.
- [33] Moshe Carmeli, *Classical Fields: General Relativity and Gauge Theory* (World Scientific Publishing Company, Singapore, 2001).
- [34] X. R. Wang, Anomalous spin hall and inverse spin Hall effects in magnetic systems, *Commun. Phys.* **4**, 55 (2021).
- [35] P. Li, J. Z. Zhang, Z. X. Guo, T. Min, and X. R. Wang, Intrinsic anomalous spin Hall effect, *Sci. China Phys. Mech. Astron.* **66**, 227511 (2023).
- [36] X. R. Wang, C. Wang, and X. S. Wang, A theory of unusual anisotropic magnetoresistance in bilayer heterostructures, *Sci. Rep.* **13**, 309 (2023).
- [37] X. R. Wang, A theory for anisotropic magnetoresistance in materials with two vector order parameters, *Chin. Phys. Lett.* **39**, 027301 (2022).
- [38] Y. Dai, Y. W. Zhao, L. Ma, M. Tang, X. P. Qiu, Y. Liu, Z. Yuan, and S. M. Zhou, Fourfold anisotropic magnetoresistance of L1₀ FePt due to relaxation time anisotropy, *Phys. Rev. Lett.* **128**, 247202 (2022).
- [39] H. Nakayama, M. Althammer, Y.-T. Chen, K. Uchida, Y. Kajiwara, D. Kikuchi, T. Ohtani, S. Geprägs, M. Opel, S. Takahashi, R. Gross, G. E. W. Bauer, S. T. B. Goennenwein, and E. Saitoh, Spin Hall magnetoresistance induced by a nonequilibrium proximity effect, *Phys. Rev. Lett.* **110**, 206601 (2013).

- [40] S. Ding, Z. Liang, D. Go, C. Yun, M. Xue, Z. Liu, S. Becker, W. Yang, H. Du, C. Wang, Y. Yang, G. Jakob, M. Kläui, Y. Mokrousov, and J. Yang, Observation of the orbital Rashba-Edelstein magnetoresistance, *Phys. Rev. Lett.* **128**, 067201 (2022).
- [41] Y. Yang, Z. Luo, H. Wu, Y. Xu, R.-W. Li, S. J. Pennycook, S. Zhang, and Y. Wu, Anomalous Hall magnetoresistance in a ferromagnet, *Nat. Commun.* **9**, 2255 (2018).
- [42] Y. Miao, D. Z. Yang, L. Jia, X. Li, S. Yang, C. X. Gao, and D. S. Xue, Magnetocrystalline anisotropy correlated negative anisotropic magnetoresistance in epitaxial $\text{Fe}_{30}\text{Co}_{70}$ thin films, *Appl. Phys. Lett.* **118**, 042404 (2021).
- [43] Y. Miao, X. Chen, S. Yang, K. Zheng, Z. Lian, Y. Wang, P. Wang, C. X. Gao, D. Z. Yang, and D. S. Xue, Non-cosine square angular-dependent magnetoresistance of the face-centered-cubic Co thin films, *J. Magn. Magn. Mater.* **512**, 167013 (2020).
- [44] R. R. Birss, *Symmetry and Magnetism* (North-Holland, Amsterdam, 1964).
- [45] P. K. Rout, I. Agireen, E. Maniv, M. Goldstein, and Y. Dagan, Six-fold crystalline anisotropic magnetoresistance in the (111) $\text{LaAlO}_3/\text{SrTiO}_3$ oxide interface, *Phys. Rev. B* **95**, 241107(R) (2017).